

Chapter 6

Petroleum Vapor Intrusion



Iason Verginelli

Abstract Petroleum vapor intrusion (PVI) is the process by which volatile petroleum hydrocarbons released from contaminated geological materials or groundwater migrate through the vadose zone into overlying buildings. PVI science showed that petroleum hydrocarbons are subjected to natural attenuation processes in the source zone and during the vapor transport through the vadose zone. Specifically, in the presence of oxygen, aerobic biodegradation typically reduces or eliminates the potential for PVI. This behavior justifies the different approach usually adopted for addressing PVI compared to less biodegradable compounds such as chlorinated solvents. In some countries, it was introduced the concept of vertical exclusion distance criteria, i.e., source to building distances above which PVI does not normally pose a concern. For buildings where the vertical separation distance does not meet screening criteria, additional assessment of the potential for PVI is necessary. These further investigations can be based on modeling of vapor intrusion, soil gas sampling, indoor measurements or preferably a combination of these to derive multiple lines of evidence. The data collected are then used for a risk assessment of the vapor intrusion pathway. This chapter provides an overview of state-of-the-science methodologies, models, benefits and drawbacks of current approaches, and recommendations for improvement.

Keywords Indoor air · LNAPL · Risk assessment · Soil gas sampling · Vapor intrusion modeling

I. Verginelli (✉)

Laboratory of Environmental Engineering, Department of Civil Engineering and Computer Science Engineering, University of Rome Tor Vergata, Via del Politecnico 1, Rome 00133, Italy
e-mail: verginelli@ing.uniroma2.it

© The Author(s) 2024

J. García-Rincón et al. (eds.), *Advances in the Characterisation and Remediation of Sites Contaminated with Petroleum Hydrocarbons*, Environmental Contamination Remediation and Management, https://doi.org/10.1007/978-3-031-34447-3_6

139

6.1 Introduction

Petroleum vapor intrusion (PVI) is the term used to describe the migration of volatile petroleum hydrocarbons (PHCs) released in the subsurface from the vadose zone into overlying buildings (Fig. 6.1). As discussed in Chap. 1, petroleum contamination can occur at various types of sites including refineries, gasoline or diesel underground storage tanks (USTs), commercial and home heating oil in aboveground storage tanks (ASTs), pipelines or oil exploration and production (E&P) sites (ITRC 2014).

PHCs in the form of light non-aqueous phase liquids (LNAPLs) tend to migrate downward in the vadose zone under the force of gravity (Rivett et al. 2011). During the vertical percolation, the LNAPL is partially retained in the pores of the formation as a relatively immobile phase due to the establishment of capillary forces (ITRC 2009) and the presence of dead-end pores as discussed in Chaps. 1 and 2. If the quantity of the release is significant, LNAPLs can reach the capillary fringe and

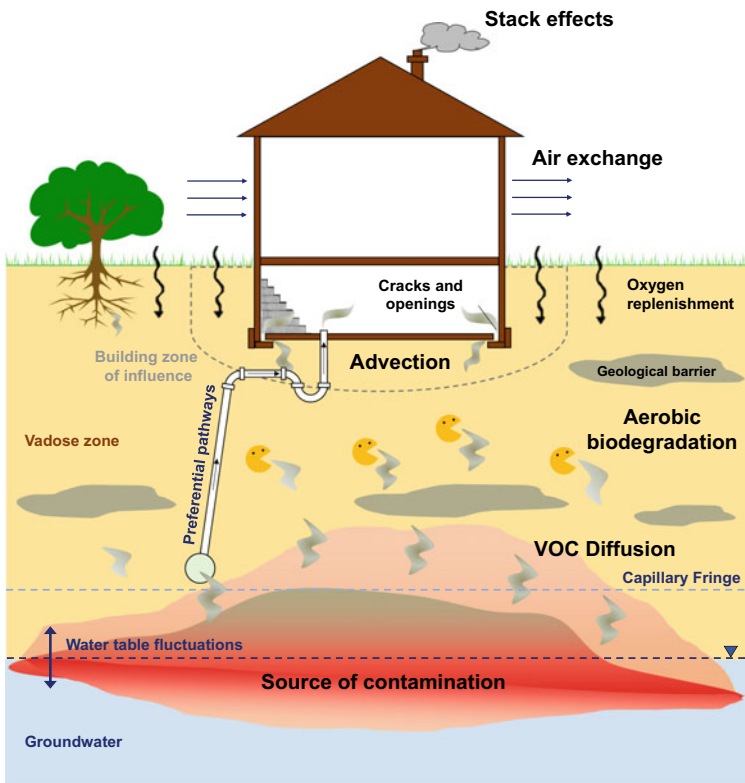


Fig. 6.1 Conceptual site model for PVI. Note that the figure is a simplified representation of the main processes involved in PVI. Subsurface environments and contaminant distributions are inherently complex and affected by dynamics such as water table fluctuations and weather effects

partially penetrate the saturated zone (U.S. EPA 1995). The LNAPL constituents in the saturated zone dissolve in groundwater generating a dissolved-phase plume downward to the source. Furthermore, the volatile constituents of LNAPL volatilize from the contaminated soil or groundwater and migrate in the subsurface mainly via diffusion and may potentially enter into the overlying buildings posing potential threats to safety (e.g., fire or explosion potential from petroleum vapors or methane) and human health (e.g., exposure to benzene from gasoline) (U.S. EPA 2015a). PHCs can be composed of hundreds of individual aromatic and aliphatic compounds. Petroleum contamination is typically assessed in terms of total petroleum hydrocarbons (TPH) with a specific focus on some individual compounds of major concern for vapor intrusion, such as BTEX (benzene, toluene, ethylbenzene, and xylenes), naphthalene, and methane (ITRC 2014). Due to its chemico-physical and toxicological properties, benzene is usually the risk driver of vapor intrusion although in some cases (e.g., gasoline contamination), C5–C8 aliphatics and C9–C12 aliphatics can contribute significantly to the overall PVI risks (Brewer et al. 2013). Furthermore, fuel additives and metabolites such as methyl tert-butyl ether (MtBE), ter-butyl alcohol (TBA), or ethylene dibromide (EDB) may also pose a risk to human health (U.S. EPA 2015a).

Advances in PVI science showed that PHCs are subjected to natural attenuation processes in the source zone and during the vapor transport through the vadose zone (ITRC 2018). It is well known that microorganisms can oxidize PHCs to carbon dioxide while utilizing electron acceptors such as molecular oxygen (Flintoft 2003; Fuchs et al. 2011) and that these microorganisms are practically ubiquitous across a wide range of subsurface conditions. In general, aerobic biodegradation rates are relatively rapid with respect to the rates of physical transport by diffusion and advection (U.S. EPA 2015a), leading to vapors attenuation by several orders of magnitude within a few meters. This behavior justifies the different approach usually adopted for addressing PVI compared to less biodegradable compounds such as chlorinated solvents.

This chapter provides an overview of the fate and transport of petroleum vapors in the subsurface and the methods available for the assessment of PVI.

6.2 Fate and Transport of Petroleum Vapors in the Subsurface

6.2.1 Natural Source Zone Depletion (NSZD)

As discussed in Chaps. 1, 5, 9, and 13, LNAPL constituents in the source zone undergo a series of naturally occurring processes that can lead to a progressive reduction of the source mass (DeVaull et al. 2020). In the early 90s, the primary mechanism attributed to the natural attenuation of LNAPL was the dissolution of the soluble constituents in groundwater and the subsequent biodegradation in the

plume (Garg et al. 2017; ITRC 2018). Later, it was found that volatilization and methanogenic biodegradation occurring within the LNAPL body and adjacent vadose and saturated zones were the main drivers of the progressive depletion of the source (Garg et al. 2017). The combination of the sorption of LNAPL constituents onto subsurface solids, dissolution into pore water, volatilization into the vadose zone, and biodegradation within the LNAPL body is usually indicated as natural source zone depletion or NSZD (API 2017; ITRC 2018). An increasing number of studies have demonstrated that significant NSZD occurs in most sites impacted by PHCs, with measured depletion rates ranging from thousands to tens of thousands of liters per hectare per year (e.g., McCoy et al. 2014; Garg et al. 2017).

6.2.2 Phase Partitioning

PHCs can be present in the subsurface as separate (LNAPL), solid (sorbed to organic matter or geological materials), liquid (dissolved in water), or gas phases. Partitioning equations can be used to calculate the chemical concentrations in these different phases.

For instance, in the presence of LNAPL, the soil gas concentration of each constituent of interest, C_{sg} (g/m^3), can be estimated using the Raoult's law (Eq. 6.1):

$$C_{sg} = S_e \cdot H \quad (6.1)$$

where H (–) is the dimensionless Henry's law constant of the contaminant of concern and S_e (mg/L), the effective contaminant solubility in LNAPL mixture (Eq. 6.2):

$$S_{e,i} = X_i \cdot S_i \quad (6.2)$$

with X_i (mol/mol) representing the mole fraction of compound i in LNAPL mixture, S_i (mg/L), the aqueous solubility of the pure-phase compound and $S_{e,i}$ (mg/L) the effective solubility of compound i in LNAPL mixture.

When LNAPL is not present, linear equilibrium partitioning can be used. For a groundwater source, the soil gas concentration, C_{sg} (g/m^3), can be derived from the liquid-phase concentration, C_w (mg/L), through Henry's law (Eq. 6.3):

$$C_{sg} = C_w \cdot H \quad (6.3)$$

In the case of vapors originating from the soil, the concentration in the vapor phase can be calculated from the total soil concentration, C_{soil} (mg/kg), assuming again a linear equilibrium partitioning (ASTM 2000) as in Eq. 6.4:

$$C_{sg} = C_{soil} \cdot K_{as} \quad (6.4)$$

Table 6.1 Chemico-physical properties of some compounds typically of interest for vapor intrusion

Compound	Molecular weight	Henry's constant	Diffusion in air	Diffusion in water	K_{oc}	Solubility
	(g/mol)	(-)	(m ² /h)	(m ² /h)	(L/kg)	(mg/L)
Benzene	78.10	0.228	3.18E-02	3.50E-06	62	1743
Toluene	92.10	0.272	3.13E-02	3.10E-06	182	526
Ethylbenzene	106.20	0.323	2.70E-02	2.81E-06	363	169
Xylenes	106.20	0.314	3.13E-02	2.81E-06	240	180
Methane	16.04	29	7.02E-02	6.16E-06	90	23
Naphthalene	128.00	0.02	2.12E-02	2.70E-06	1549	31

with K_{as} (kg/L) being given by Eq. 6.5:

$$K_{as} = \frac{\rho_s \cdot H}{\theta_w + K_{oc} \cdot f_{oc} \cdot \rho_s + H \cdot \theta_a} \quad (6.5)$$

where ρ_s (kg/L) is the soil bulk density, θ_w (cm³/cm³) the moisture content of the soil, θ_a (cm³/cm³) the air-filled porosity, K_{oc} (L/kg) the organic carbon to water partition coefficient, and f_{oc} (g/g) the organic carbon fraction of the soil.

Table 6.1 reports the chemico-physical properties of petroleum compounds typically of interest for vapor intrusion.

An example of phase partitioning for benzene is depicted in Figs. 6.2 and 6.3. The two figures show the soil gas concentrations estimated for benzene as a function of groundwater and soil concentrations, respectively. For groundwater, the soil gas concentrations were estimated using the equations described before at the water table interface and above the capillary fringe (calculated with the attenuation factor AF_{cap} discussed in the next section for a sandy soil with the soil properties reported in Table 6.2). For the soil contamination, the soil gas concentrations were estimated for a sandy soil (see Table 6.2), assuming various contents of the f_{oc} .

This example shows that, depending on the extent of the contamination, the concentration of benzene in soil gas varies in the order of magnitude ranging from less than 1 to tens of g/m³. Note that in the case of a diesel or gasoline contamination, the BTEXs constitute only a small fraction of TPH (fraction of percent to few percent in mass), and thus, the effective solubility and saturation concentration in the soil of benzene (and consequently the maximum soil gas concentrations) can be lower (see Eq. 6.2) than the upper-bound values reported in these figures.

6.2.3 Molecular Diffusion

Diffusion is typically the dominant transport mechanism of vapors in the vadose zone (ITRC 2018). Molecular diffusion is the movement of a chemical from an area of

Fig. 6.2 Soil gas concentration for benzene estimated as a function of groundwater concentration at the water table interface and above the capillary fringe assuming a sandy soil and a groundwater depth at 3 m below ground surface

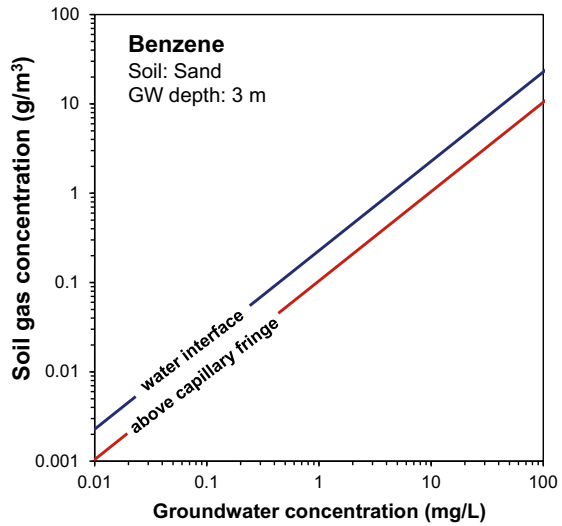
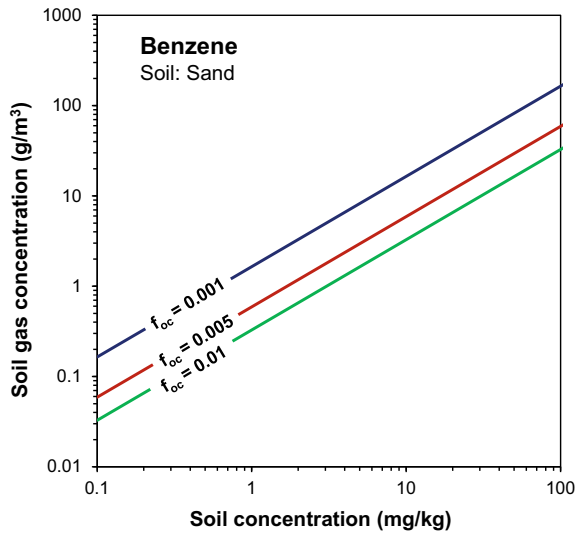


Fig. 6.3 Soil gas concentrations for benzene estimated as a function of soil concentration and f_{oc} for benzene assuming a sandy soil



higher concentration to an area of lower concentration. Diffusion occurs in both the aqueous and gas phases. The diffusive mass flux is directly proportional to the soil vapor concentration gradient. Thus, the higher the soil vapor concentrations in the source zone, the higher the flux.

Table 6.2 Soil properties (U.S. EPA 2017)

SCS soil type	ρ_s	θ_T	θ_w	$\theta_{w, \text{cap}}$	θ_r	h_{cap}	m	α	Permeability to vapor flow (k_v)
	kg/L	(-)	(-)	(-)	(-)	cm	(-)	(1/cm)	(cm^2)
Sand	1.66	0.375	0.054	0.253	0.053	17	0.685	0.035	9.91E-08
Loamy Sand	1.62	0.390	0.076	0.303	0.049	19	0.427	0.035	1.55E-08
Sandy Loam	1.62	0.387	0.103	0.320	0.039	25	0.310	0.027	5.34E-09
Sandy Clay Loam	1.63	0.384	0.146	0.333	0.063	26	0.248	0.021	1.75E-09
Loam	1.59	0.399	0.148	0.332	0.061	38	0.321	0.011	1.58E-09
Silt Loam	1.49	0.439	0.180	0.349	0.065	68	0.399	0.005	2.25E-09
Clay Loam	1.48	0.442	0.168	0.375	0.079	47	0.294	0.016	1.09E-09
Silty Clay Loam	1.37	0.482	0.198	0.399	0.090	134	0.343	0.008	1.43E-09
Silty Clay	1.38	0.481	0.216	0.424	0.111	192	0.243	0.016	1.25E-09
Silt	1.35	0.489	0.167	0.382	0.050	163	0.404	0.007	5.60E-09
Sandy Clay	1.63	0.385	0.197	0.355	0.117	30	0.172	0.033	1.46E-09
Clay	1.43	0.459	0.215	0.412	0.098	82	0.202	0.015	1.86E-09

The diffusive mass flux of a vapor in the soil, J_{diff} (g/m²/h), is described by Fick's law:

$$J_{\text{diff}} = -D^{\text{eff}} \frac{dC}{dz} \quad (6.6)$$

where dC/dz (g/m⁴) is the concentration gradient, and D^{eff} (m²/h) the effective diffusion coefficient of the constituent in the porous medium.

The moisture content in the formation strongly affects the rate of the diffusive mass flux through the vadose zone. Diffusion coefficients in water are indeed about three to four orders of magnitude lower than the diffusion coefficients in air (see Table 6.1). Thus, as the moisture content in the formation increases, the diffusive flux decreases (ITRC 2018).

Another factor that can influence the diffusion coefficients is the subsurface temperature. In this case, as the temperature increases, the diffusive flux increases (Unnithan et al. 2021). Note that an increase in subsurface temperature also increases the Henry's law constant and the vapor pressure, thus affecting the phase partitioning of the contaminant in the subsurface.

Several equations were derived to relate the effective diffusion coefficient to the free-air diffusion coefficient of the compound and soil characteristics (Tillman and Weaver 2005). Typically, in vapor intrusion studies, the empirical equation derived by Millington and Quirk (1961) as reported by Johnson and Ettinger (1991) is used (Eq. 6.7):

$$D^{\text{eff}} = D_{\text{air}} \cdot \frac{\theta_a^{10/3}}{\theta_T^2} + \frac{D_{\text{wat}}}{H} \cdot \frac{\theta_w^{10/3}}{\theta_T^2} \quad (6.7)$$

where D_{air} (m^2/h) and D_{wat} (m^2/h) are the diffusion coefficients in air and water, respectively, and θ_T (cm^3/cm^3) is the soil porosity.

Considering that the vertical moisture content profile through the soil is not constant, the overall diffusion coefficient in the vadose zone can be calculated by discretizing the system in n layers as suggested by Johnson and Ettinger (1991):

$$D_{\text{tot}}^{\text{eff}} = \frac{L}{\sum_i^n \frac{d_i}{D_i^{\text{eff}}}} \quad (6.8)$$

where L (m) is the depth of source zone from the building foundations, d_i (m) the thickness of the i th layer, and D_i^{eff} (m^2/h) the associated diffusion coefficient calculated considering the moisture content of this layer.

In cases involving homogenous soil, the moisture vertical profile can be estimated using the van Genuchten (1980) equation (Eq. 6.9):

$$S_w(z) = S_{wr} + (1 - S_{wr}) \cdot \left[\frac{1}{1 + (\alpha \cdot z)^m} \right]^m \quad (6.9)$$

with:

$$S_w = \frac{\theta_w}{\theta_T} \quad (6.10)$$

$$S_{wr} = \frac{\theta_r}{\theta_T} \quad (6.11)$$

$$m = 1 - 1/n \quad (6.12)$$

where z (cm) is the distance from the water table, θ_r (cm^3/cm^3) is the residual soil water content, and α (1/cm), m (-), and n (-) are the van Genuchten curve shape parameters (Table 6.2).

Therefore, in the capillary fringe, the diffusive vapor flux is relatively low compared to the one expected in the vadose zone. To estimate the attenuation factor in the capillary fringe, AF_{cap} (-), i.e., the ratio of the volatile organic compound (VOC) concentration at the top of the capillary fringe, C_{cap} (g/m^3), to the VOC concentration in the soil gas in correspondence of the source in groundwater, C_{source} (g/m^3), a two-layer model can be applied (U.S. EPA 2017). For instance, the attenuation factor in the capillary fringe can be estimated using Eqs. 6.13 and 6.14 (Verginelli and Baciocchi 2014):

$$\text{AF}_{\text{cap}} = \frac{C_{\text{cap}}}{C_{\text{source}}} \approx \left(1 - \frac{h_{\text{cap}}}{L} \right) \cdot \frac{D_{\text{tot}}^{\text{eff}}}{D_{\text{soil}}^{\text{eff}}} \quad (6.13)$$

with:

$$D_{\text{tot}}^{\text{eff}} = \frac{L}{\frac{h_{\text{cap}}}{D_{\text{cap}}^{\text{eff}}} + \frac{L-h_{\text{cap}}}{D_{\text{soil}}^{\text{eff}}}} \quad (6.14)$$

where h_{cap} (m) is the thickness of the capillary fringe, D_{cap} (m^2/h) and D_{soil} (m^2/h) are, respectively, the effective diffusion coefficients in the capillary fringe and in the vadose zone calculated with Eq. 6.7 with the moisture content in the vadose zone and in the capillary fringe specific of the type of sediment considered in the site (see Table 6.2).

Note that this two-layer approach provides a conservative estimate of the attenuation through the capillary fringe. Indeed, by considering the vertical moisture profile obtained with the van Genuchten (1980) equation, the attenuation can result up to two orders of magnitude higher than the one calculated with the two-layer model approach (Hers et al. 2003; Shen et al. 2013; Yao et al. 2017, 2019).

6.2.4 Advection and Bubble-Facilitated Transport (Ebullition)

Advection is the transport mechanism by which soil gas moves due to pressure differences. The advective flux, J_{adv} ($\text{g}/\text{m}^2/\text{h}$), from a source zone with a known C_{sg} (g/m^3) can be estimated with Eq. 6.15:

$$J_{\text{adv}} = C_{\text{sg}} \cdot v \quad (6.15)$$

where v (m/h) is the advective velocity that can be calculated according to Darcy's law (Eq. 6.16):

$$v = \frac{k_v}{\mu_g} \cdot \frac{\Delta P}{L} \quad (6.16)$$

where k_v (m^2) is the formation permeability to vapor flow, μ_g (Pa h) is the vapor viscosity, and ΔP (Pa) is the pressure difference along a distance L (m).

In open ground conditions, the pressure differences can be generated by barometric pumping caused by ambient pressure and temperature variation and are usually limited to shallow depths (McHugh and McAlary 2009; Eklund 2016).

Pressure gradients between the air inside a building and the subsurface can be caused by several processes such as wind loading on the building, heating, ventilation, and air conditioning (HVAC) operation or the stack effect caused by heating of building air to temperatures higher than outdoor air (ITRC 2014). Thus, in the zone very close to a basement or a foundation, advective transport is likely to be the most significant contribution to PVI, as soil gases are generally swept into the building

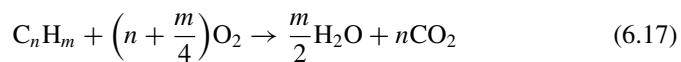
through foundation cracks due to the indoor–outdoor building pressure differential (U.S. EPA 2015b). Typically, pressure differentials between the building and the subsurface are relatively small (a few Pascals), so the building zone of influence of the pressure fields associated with the building-induced advective flow on soil gas flow is usually less than 1 m, vertically and horizontally (ITRC 2014; U.S. EPA 2015b; Ma et al. 2020a).

Advection may become important also at depth due to water table fluctuation (Tillman and Weaver 2007; Illangasekare et al. 2014; Liu et al. 2021) and near to the LNAPL source zone when the rate of gas production from methanogenesis is high (Ma et al. 2012; Yao et al. 2015). For instance, Molins et al. (2010) estimated that at the Bemidji site, advection was responsible for approximately 15% of the net flux of methane. Additionally, if methanogenesis is occurring in the saturated zone, then, after the groundwater becomes super-saturated with gas, bubble formation can occur, leading to gas transport to the vadose zone (Amos et al. 2005; Amos and Mayer 2006). Bubble formation is termed degassing. Bubble transport of gas from groundwater to the vadose zone is termed ebullition and occurs episodically (Sihota et al. 2013) along fractures in the formation. In this case, as shown by Soucy and Mumford (2017) and Ma et al. (2019), the mass flux of VOC transport could be up to two orders of magnitude higher than that of diffusive VOC transport.

6.2.5 Biodegradation During Vapor Transport

In the unsaturated zone, PHCs are readily degraded to carbon dioxide (CO₂) in the presence of oxygen (O₂) by subsurface microorganisms.

The mineralization reaction under aerobic conditions of a generic hydrocarbon C_nH_m can be written as in Eq. 6.17:



From Eq. 6.17 and as indicated by Eq. 6.18, the mass ratio of O₂ consumption to the generic hydrocarbon C_nH_m mineralized is equal to:

$$\gamma = \left(n + \frac{m}{4}\right) \cdot MW_{O_2} / MW_{C_nH_m} \quad (6.18)$$

For many hydrocarbons of interest for vapor intrusion (e.g. benzene), this mass ratio is approximately 3 g_{O₂}/g_{C_nH_m} (ITRC 2018).

Anaerobic degradation with other electron acceptors (e.g., nitrate or sulfate) can also occur with PHCs, but is usually neglected as there is no ready source for replenishment of these electron acceptors (ITRC 2014). Note that while aerobic biodegradation is the primary mechanism in the unsaturated zone, in the LNAPL source zone, as discussed earlier, PHCs typically degrade under methanogenic conditions with consequent production of methane and carbon dioxide (ITRC 2018).

There have been extensive compilations of rates of aerobic degradation for PHCs (e.g., DeVaul et al. 1997; Hers et al. 2000; Ririe et al. 2002; Davis et al. 2009a; DeVaul 2011). Typically, in PVI studies, first-order, water-phase aerobic degradation rates are considered. For instance, a compilation of first-order water phase biodegradation rate statistics from laboratory and field studies was reported by DeVaul (2011). Table 6.3 reports an extract of this study for some VOCs typically of concern. For more details, readers are directed to the original reference (DeVaul 2011).

Assuming a diffusion-dominated transport and first-order biodegradation, the attenuation factor due to biodegradation, AF_{bio} (-), i.e., the ratio of the VOC concentration at the top of the aerobic zone, C_{ss} (g/m^3), to the VOC concentration at the aerobic to the anaerobic interface, C_a (g/m^3), can be calculated as in Eq. 6.19 (ITRC 2014; Verginelli and Baciocchi 2021):

$$AF_{\text{bio}} = \frac{C_{\text{ss}}}{C_a} = \exp\left(-\frac{L_a}{L_R}\right) \quad (6.19)$$

where L_a (m) is the thickness of the aerobic zone, and L_R (m) is the diffusive reaction length as defined by Eq. 6.20:

$$L_R = \sqrt{\frac{D^{\text{eff}} \cdot H}{\lambda \cdot \theta_w}} \quad (6.20)$$

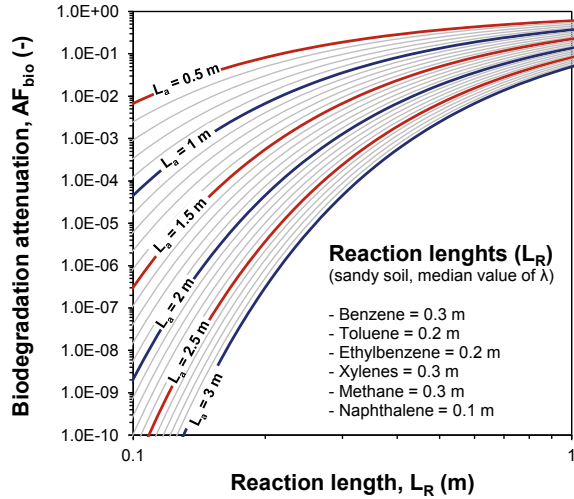
where λ (1/h) is the first-order reaction rate constant, θ_w (cm^3/cm^3) is the moisture content of the formation, D^{eff} (m^2/h) is the effective diffusion coefficient in the vadose zone, and H (-) is the dimensionless Henry's law constant.

The biodegradation attenuation factors calculated with the above equation as a function of the reaction length (L_R) and the thickness of the aerobic zone (L_a) are shown in Fig. 6.4. The reaction lengths expected in a sandy soil (see Table 6.2) for petroleum vapors of interest considering the median value of literature biodegradation rate constants (DeVaul 2011) are also reported in Fig. 6.4 as a reference. It can be

Table 6.3 First-order water phase biodegradation rates under aerobic conditions of some petroleum compounds typically of interest for vapor intrusion (DeVaul 2011 as reported by ITRC 2014)

Compound	First-order water phase biodegradation rates (h^{-1}) under aerobic conditions		
	Median value	Interquartile (1st to 3rd quartiles)	Data range (minimum to maximum)
Benzene	0.27	0.087–0.78	0.028–3
Toluene	0.72	0.19–1.4	0.028–77
Ethylbenzene	0.79	0.31–1.4	0.072–6.6
Xylenes	0.27	0.089–0.64	0.045–14
Methane	88	50–100	0.31–190
Naphthalene	0.12	0.054–5	0.021–9.8

Fig. 6.4 Biodegradation attenuation factor calculated as a function of the reaction length (L_R) and thickness of the aerobic zone (L_a). As reference in the is are reported the reaction length that can be expected in sandy soil for petroleum vapors of interest considering the median value of literature biodegradation rate constants (DeVaul 2011)



noticed that for the typical reaction lengths expected for the compounds of concern, a few meters of clean aerobic soil can ensure an attenuation in the vapor concentrations of several orders of magnitude.

The thickness of the aerobic zone, L_a (m), at the center of the building can be calculated using the expression derived by Verginelli et al. (2016a) to account for the building footprint (see Eqs. 6.21–6.23):

$$L_a = L - \frac{L}{\pi} \arccos \left[1 + \frac{\cos(\pi \cdot w_a) - 1}{\Omega} \right] \quad (6.21)$$

with:

$$\Omega = \frac{1}{\cosh^2\left(\frac{\pi \cdot L_{\text{slab}}}{4L}\right)} \quad (6.22)$$

$$w_a = \frac{\frac{L_b/L_{R,i}}{1+L_b/L_{R,i}}}{1 + \frac{D_{\text{ox}}(C_{\text{ox}}^{\text{atm}} - C_{\text{ox}}^{\text{min}})}{\sum \gamma_i \cdot D_i^{\text{eff}} \cdot C_i^s} \left(1 - \frac{d_f}{d_s - L_b}\right)} \quad (6.23)$$

where $C_{\text{ox}}^{\text{atm}}$ (g/m^3) is the atmospheric oxygen concentration (e.g., 21% v/v), $C_{\text{ox}}^{\text{min}}$ (g/m^3) is the minimum oxygen concentration (e.g., 1% v/v), C_i^s (g/m^3) is the petroleum vapor source concentration, γ_i (g/g) is the stoichiometric mass of oxygen consumed per mass of hydrocarbon i reacted, d_s (m) is the vertical source distance from open ground, d_f (m) is the slab depth from open ground, L_b (m) is the anaerobic zone thickness, $L_{R,i}$ (m) is the diffusive reaction length of hydrocarbon i and D (m^2/h) is the effective porous medium diffusion coefficients for the different species. Note

that in the case of a hydrocarbons mixture, all the degradable compounds present in the source should be included.

6.2.6 *Entry into the Building: Traditional and Preferential Pathways*

Vapor intrusion can occur through different entry points in the building floors, walls, foundations, or through preferential pathways. The traditional vapor intrusion pathway refers to the entry of the VOCs from the subsurface through cracks, openings, and gaps in the basement (U.S. EPA 2015b). The intruded vapors into the building can mix and dilute with indoor air due to HVAC systems or windows opening. Dilution of sub-slab soil vapor concentrations is hence characterized by the building ventilation rate that is typically expressed as air exchanges per hour (AER).

For these scenarios, the sub-slab to indoor air attenuation factor, AF_{ss} (-), i.e., the ratio of the VOC concentration in indoor air, C_{indoor} (g/m^3), to the VOC concentration in the sub-slab, C_{ss} (g/m^3), can be expressed as the ratio of the soil gas entry rate, Q_{soil} (m^3/h), to the building ventilation rate, $Q_{building}$ (m^3/h), as it is shown in Eq. 6.24:

$$AF_{ss} = \frac{C_{indoor}}{C_{ss}} = \frac{Q_{soil}}{Q_{building}} = \frac{Q_{soil}}{AER \cdot V_{building}} \quad (6.24)$$

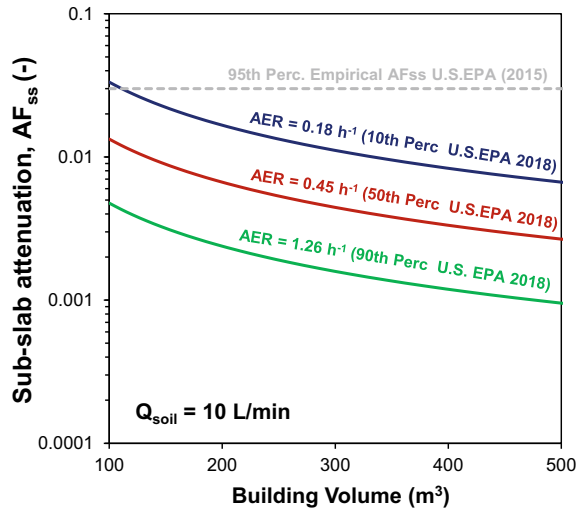
where AER (1/h) is the air exchange rate, and $V_{building}$ (m^3) is the building volume.

Alternatively, for a screening purpose, U.S. EPA (2015b) proposed an empirical sub-slab to indoor air attenuation factor of 0.03 that represents the upper-bound value of empirical datasets. Note that the representativeness of this empirical attenuation factor proposed by U.S. EPA has been the subject of much debate (Song et al. 2011; Brewer et al. 2014; Yao et al. 2018; Lahvis and Ettinger 2021).

The sub-slab attenuation factor (AF_{ss}) calculated with Eq. 6.24 as a function of the air exchange rate (AER) and the building volume ($V_{building}$), assuming a soil gas entry rate of 10 L/min (i.e., the upper bound of the values of Q_{soil} indicated by U.S. EPA 2002) is shown in Fig. 6.5. From Fig. 6.5, it can be observed that the 0.03 value of AF_{ss} is very conservative as it can be considered representative of an air exchange rate of $0.18 h^{-1}$ (i.e., the 10th percentile of the values reported by U.S. EPA 2018), a soil gas entry rate of 10 L/min (i.e., the upper bound of the values of Q_{soil} indicated by U.S. EPA 2002) and a building volume of $100 m^3$ (i.e., a building area of $40 m^2$ considering a building mixing height of 2.5 m for a slab-on-grade scenario).

Instead, preferential pathways are specific migration routes that can cause higher contaminant flux into a building compared to the average transport through the formation (Nielsen and Hvidberg 2017; Beckley and McHugh 2020; Unnithan et al. 2021).

Fig. 6.5 Sub-slab attenuation factor ($AF_{ss} = Q_{soil}/Q_{building}$) as a function of the building volume ($V_{building}$) and of the air exchange rate (AER) for different values of the soil gas entry rate (Q_{soil})



For instance, sewer pipes and other utility conduits (e.g., fiber optics, cable television, and telephone cables) are preferential pathways that can result in vapor intrusion when VOC vapors migrate through the interior of the conduits into buildings (McHugh et al. 2017; Roghani et al. 2018). According to the data collected by Beckley and McHugh (2020) from more than 30 sites across the United States, the magnitude of vapor attenuation from the sewer into the buildings is often large ($> 1000\times$ attenuation) although building-specific plumbing faults can result in much lower vapor attenuation ($<100\times$). The authors concluded that, in general, sites with a higher risk for sewer vapor intrusion are those with direct interaction between the subsurface VOC source (e.g., groundwater) and the sewer line.

Although less investigated, a high permeability region in the vadose zone (e.g., gravel layers or fractured rocks) or the tree roots system can also act as preferential pathways for the vapor migration in the subsurface (Unnithan et al. 2021).

6.3 PVI Assessment

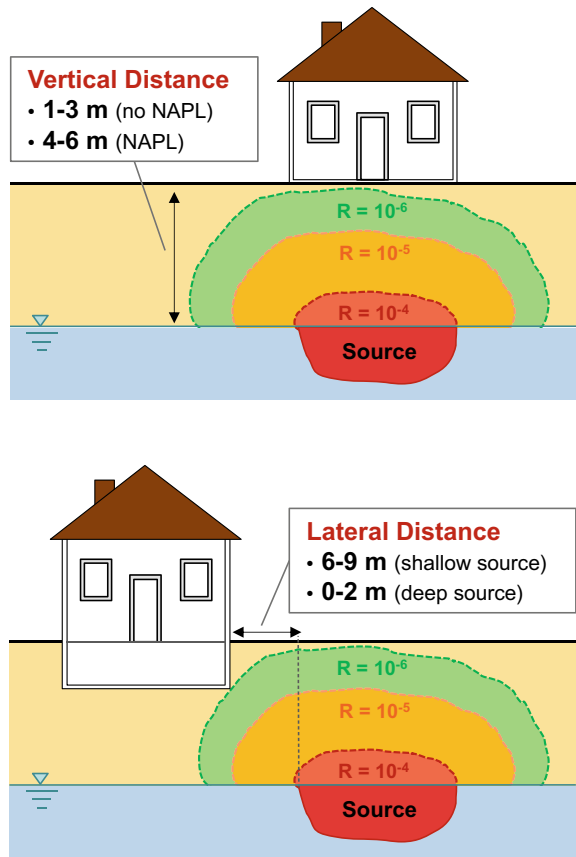
6.3.1 Vertical and Lateral Exclusion Distance

Source to building distance criteria can be applied to screen the vapor intrusion pathway. If the building is closer to the source than the screening distance, then further evaluations are recommended (Ma et al. 2020a). For instance, a source to building distance of 30 m (100 ft) has been used in different countries for both lateral and vertical distance-based screening since the early 2000s.

For petroleum vapor intrusion, shorter distances can be adopted due to PHCs biodegradation within the vadose zone (Fig. 6.6). For instance, Davis et al. (2009b) analyzed more than two hundred vapor samples estimating that 1.5 m (5 ft) and 10 m (30 ft) thickness of clean soil is sufficient to attenuate PHC vapors from dissolved-phase and LNAPL sources to non-detectable levels, respectively. Later, McHugh et al. (2010) proposed a separation distance of 3 m (10 ft) for petroleum vapors resulting from dissolved-phase groundwater sources and a separation distance of 10 m (30 ft) for LNAPL vapor sources. Lahvis et al. (2013) have estimated a separation distance at petroleum UST sites of 4 m (13 ft) for LNAPL sources, whereas for dissolved-phase vapor sources, the probability of detecting benzene vapor above the screening level of $30 \mu\text{g}/\text{m}^3$ was found to be below 5%. Similar values were also reported by U.S. EPA (2013) where, depending on the method adopted for the data interpretation (i.e., vertical distance method or clean soil method), screening distances of 0 to 1.6 m (5.4 ft) for dissolved-phase sources (benzene groundwater concentration below 1 mg/L and benzene soil gas screening level of $100 \mu\text{g}/\text{m}^3$) and 4.1–4.6 m (13.5–15 ft) for LNAPL sources at UST sites and 5.5–6.1 m (18–20 ft) for LNAPL sources at non-UST sites were defined. CRC CARE (2013) has also determined vertical screening distances of 1.5 m for dissolved phase and 3–5.6 m for LNAPL sources (note that these values are the ones reported in the document not considering the 1.5-fold uncertainty factor). These empirical screening distances are also supported by mathematical modeling. For instance, results from numerical (Hers et al. 2000; Abreu and Johnson 2006; Abreu et al. 2009; Hers et al. 2014) and analytical models (DeVaull 2007; Yao et al. 2014; Verginelli and Baciocchi 2014) were consistent with the empirical exclusion distance values reported above, showing that, in nearly all cases, source to building vertical separation distances greater than 2 m or 5 m are sufficient to attenuate to acceptable risk-based levels PHC vapors from dissolved-phase or LNAPL sources, respectively. For the lateral source to building exclusion distance, Verginelli et al. (2016b) estimated that 6 and 9 m lateral distances are sufficient to attenuate petroleum vapors below risk-based values for groundwater and soil sources, respectively. Note that these screening criteria were derived assuming that preferential pathways are not present.

A key aspect to be evaluated for the applicability of these distance criteria is the establishment of oxygenated zones beneath large buildings (Abreu et al. 2013). A building slab can potentially act as a surface cap reducing the migration of oxygen into the soil beneath the building and, consequently, limiting the attenuation of vapor concentrations due to aerobic biodegradation (Knight and Davis 2013). In most PVI conceptual site models, atmospheric oxygen at the ground surface beyond the building perimeter is considered the primary source of oxygen in the subsurface (Abreu and Johnson 2006; Abreu et al. 2009). Verginelli et al. (2016a) developed an analytical solution (Eq. 6.25) to predict the critical slab size, $L_{\text{slab,c}}$ (m), normalized to the source to building vertical distance, L (m), above which the development of an “oxygen shadow” (i.e., anoxic zone) at the center of the impervious building is expected:

Fig. 6.6 Typical vertical and lateral source to building distance criteria adopted for petroleum vapor intrusion that ensure an acceptable risk (e.g., a carcinogenic risk, R , equal to 10^{-6}). Note that these screening criteria are set assuming that preferential pathways are not present

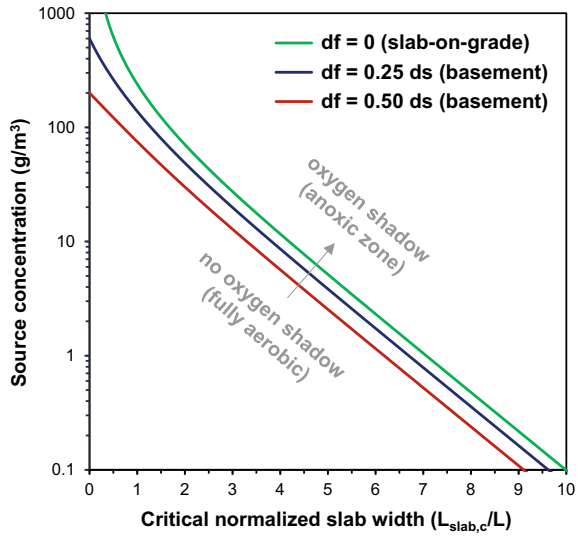


$$\frac{L_{\text{slab},c}}{L} = \frac{4}{\pi} \ln \left[\cot \left(\frac{\pi \cdot w_a}{4} \right) \right] \tag{6.25}$$

with w_a (–) defined as reported in Eq. 6.23.

The critical slab width to source depth ratio ($L_{\text{slab},c}/L$) calculated with the above equation as a function of the vapor source concentration for a slab-on-grade ($d_f = 0$) and two basement scenarios ($d_f = 0.25d_s$ and $d_f = 0.5d_s$) is shown in Fig. 6.7. The establishment of an oxygen shadow at the center of the building depends on the source depth and vapor source concentration. For instance, for a vapor source concentration of 100 g/m^3 and a source depth of 10 m, an oxygen shadow at the center of buildings larger than 15 m (slab-on-grade, $L_{\text{slab},c}/L \approx 1.5$) or 5 m (basement, $L_{\text{slab},c}/L \approx 0.5$) is expected, i.e., highlighting that vertical screening criteria cannot be applied and further investigations might be needed to evaluate the sub-slab oxygen conditions. Note that the establishment of an oxygenated zone beneath impervious slabs is relatively insensitive to the type of formation as the oxygen replenishment from open ground linearly depends on the ratio of the diffusion coefficients of oxygen

Fig. 6.7 Critical normalized building slab size ($L_{slab,c}/L$) above which the development of an oxygen shadow is expected at the center of the building calculated with the solution derived by Verginelli et al. (2016a)



and vapor into the soil that for the different types of soil remains almost constant (Knight and Davis 2013; Verginelli et al. 2016a).

6.3.2 Analytical and Numerical Modeling

When the distance criteria discussed in the previous section are not satisfied or are not applicable (e.g., large buildings for which an oxygen shadow is expected), the indoor concentrations, C_{indoor} (g/m^3), can be estimated through mathematical modeling based on the concentrations detected in the source (Eq. 6.26):

$$\begin{cases} C_{indoor} = C_{gw} \cdot H \cdot AF_{cap} \cdot AF_{bio} \cdot AF_{ss} \text{ (groundwater)} \\ C_{indoor} = C_{soil} \cdot K_{as} \cdot AF_{bio} \cdot AF_{ss} \text{ (soil)} \end{cases} \quad (6.26)$$

The different parameters in Eq. 6.26 were already discussed in the previous sections.

As shown by Yao et al. (2013), Bekele et al. (2013) and Verginelli and Yao (2021), in the last decades, there have been numerous analytical (e.g., Johnson and Ettinger 1991; Parker 2003; DeVaul 2007; Davis et al. 2009a; Verginelli and Baciocchi 2014; Yao et al. 2014, 2015, 2016a; Verginelli et al. 2016a) and numerical models (Hers et al. 2000; Abreu and Johnson 2006; Abreu et al. 2009; Hers et al. 2014) to simulate the migration of subsurface volatile organic compounds into the building of concern and that can be used for the estimation the attenuation factors reported in the above equation. Among these, the Johnson and Ettinger (1991) model is the most

widely used algorithm for assessing the vapors intrusion into enclosed spaces for non-biodegradable compounds and is incorporated in many risk assessment standards (e.g., ASTM E2081-00). For petroleum vapors, the BioVapor tool (DeVaul et al. 2010) is commonly used. BioVapor incorporates the 1-D analytical solution derived by DeVaul (2007) based on a mass continuity among upward diffusive flux, entry rate through the foundation and indoor exchange rate of hydrocarbons, and accounts for oxygen limited biodegradation. Alternatively, to evaluate the petroleum vapors and oxygen 2-D profile below the building foundations, the PVI2D tool (Verginelli et al. 2016c) can be used. PVI2D incorporates the analytical model developed by Yao et al. (2016a) and can be used to provide 2-D soil gas concentration profiles for both hydrocarbon and oxygen, based on coupled oxygen-hydrocarbon transport and reaction besides source-to-indoor air concentration attenuation factors. An example of the benzene and oxygen soil gas concentration profiles simulated using the PVI2D tool is shown in Fig. 6.8. In this example, a benzene vapor source concentrations of 50 g/m^3 , a sandy soil (Table 6.2), and a biodegradation rate of 0.27 h^{-1} are assumed. As shown by Yao et al. (2016b), for homogenous site conditions, PVI2D provides soil gas concentration profiles and source-to-indoor air attenuation factors similar to the ones obtained using the more sophisticated numerical model developed by Abreu and Johnson (Abreu and Johnson 2006; Abreu et al. 2009).

For complex contamination scenarios involving transient transport, soil heterogeneities, preferential pathways, and non-uniform sources, numerical modeling is needed. In PVI field, the Abreu and Johnson's model is the reference model by the majority of practitioners and has been employed in almost all U.S. EPA's PVI technical documents (Abreu and Schuver 2012; Abreu et al. 2013) since its publication.

It is worth noting that, especially in potentially critical scenarios (e.g., NAPL sources), mathematical modeling should be used as one of the lines of evidence for PVI assessment in conjunction with site investigation data as part of a multiple-lines-of-evidence approach (U.S. EPA 2015b). Indeed, mathematical modeling may not reflect all of reality as subsurface heterogeneity (e.g., geological barriers, fractured soils, plants roots), preferential pathways, or barometric pumping cycling can hardly be schematized and predicted (Unnithan et al. 2021). Besides, for their simplicity, in most cases, practitioners prefer 1D models compared to more sophisticated 2D and 3D models leading to a further oversimplification of the processes that can affect the transport of petroleum vapors in the subsurface and the consequent intrusion into the building.

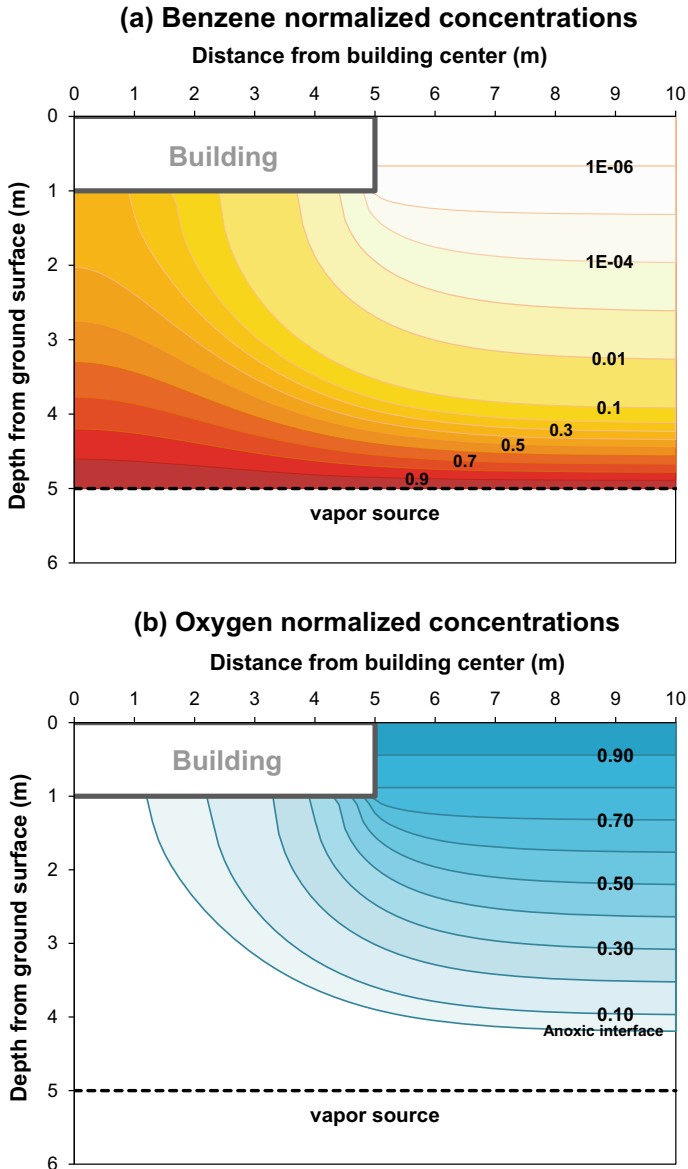


Fig. 6.8 Example of benzene and oxygen soil gas concentration profiles simulated with PVI2D (Verginelli et al. 2016c; Yao et al. 2016a) for a basement scenario. In this example, a benzene vapor source concentrations of 50 g/m³, a sandy soil (Table 6.2), and a biodegradation rate of 0.27 h⁻¹ are assumed. The hydrocarbons and oxygen soil gas concentrations are normalized to source concentration and atmosphere concentration, respectively

6.3.3 Soil Gas Sampling

Measurement of soil gas is a common approach for evaluating the vapor intrusion pathway. Soil gas data compared to soil matrix and groundwater data represent a direct measurement of the contaminant that can potentially migrate into indoor air. Soil gas sampling is usually carried out by installing temporary or permanent probes into the subsurface (U.S. EPA 2015b) as illustrated in Fig. 6.9. These probes are typically equipped with active sampling systems that pump out the air-filled porosity of the soil, and the vapor samples are collected using Tedlar® bags, passivated stainless-steel canisters, or sorbent tubes (e.g., automated thermal desorption tubes). The samples are then sent to the laboratory for the VOCs analyses. Over recent years, passive samplers have become an attractive alternative option for the monitoring of soil gas. Passive sampling is based on the molecular diffusion of the compounds from the subsurface to a collecting medium in response to a chemical potential difference (Górecki and Namiesnik 2002). Passive sampling has potential advantages over conventional active methods, including simpler protocols, smaller size for ease of shipping and handling, and lower costs (McAlary et al. 2014; Salim and Górecki 2019). A wide variety of “linear uptake” passive samplers have been designed and tested for soil gas, including Petrex tubes, Emflux® cartridges, Beacon B-Sure Samples™, Gore™ Modules, and PDMS membranes (Hodny et al. 2009; McAlary et al. 2014; Liang et al. 2020). Each of these methods provides results in units of the mass of contaminant adsorbed over the exposure duration and then the correlation between the mass adsorbed and the soil vapor concentration can be quantitatively assessed based on specific uptake rates. The uptake rate is the key parameter for a quantitative assessment of soil gas concentration by passive samplers, and it depends on the environmental conditions (e.g., subsurface temperature, humidity, and pressure) and on the geometry of the sampling device and the sorbent characteristics (McAlary et al. 2014). Alternatively, “equilibrium” passive samplers based on polymers were recently proposed. For instance, Gschwend et al. (2022) investigated the use of thin, low-density polyethylene (PE) films as the sampling absorbent for estimating the soil gas concentrations of BTEX and chlorinated solvents.

Soil gas samples can be differentiated by the location of the samples. Near-slab soil gas samples are collected outside a structure but within a short distance (a few meters) of the building’s perimeter. Soil gas samples collected at higher distances from the perimeter of the building are referred to as exterior soil gas samples and can be useful for delineating the vapor plume, for screening areas for subsequent indoor sampling or for the evaluation of future vapor intrusion scenarios. Finally, sub-slab soil gas samples are collected from the subsurface immediately under the building foundation or slab.

As indicated by Eq. 6.27, based on the concentrations detected in soil gas, the vapor intrusion pathway is evaluated through the application of the sub-slab to indoor air attenuation factor, AF_{ss} (–), in the case of sub-slab sampling or considering also the biodegradation attenuation factor, AF_{bio} (–), in the case of soil gas data collected at some depth from the building zone:

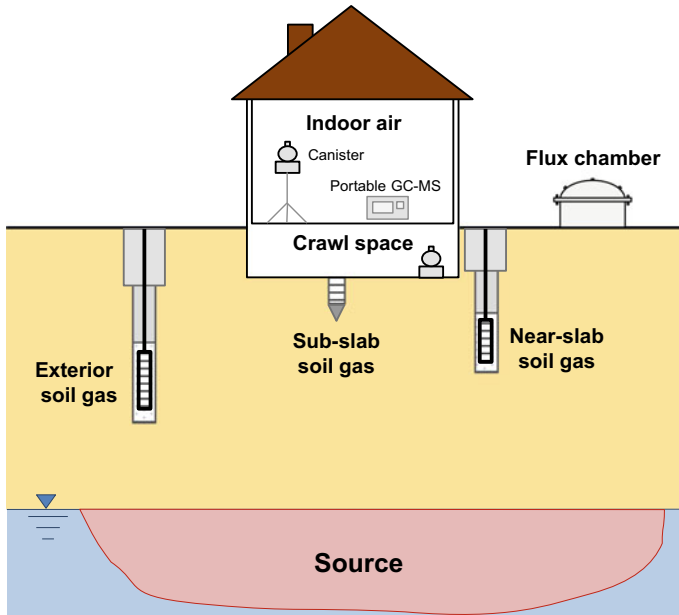


Fig. 6.9 Soil gas, flux chamber, and indoor air sampling

$$\begin{cases} C_{\text{indoor}} = C_{\text{sg}} \cdot \text{AF}_{\text{ss}} \text{ (sub-slab)} \\ C_{\text{indoor}} = C_{\text{sg}} \cdot \text{AF}_{\text{bio}} \cdot \text{AF}_{\text{ss}} \text{ (deep soil gas)} \end{cases} \quad (6.27)$$

Alternatively, or in conjunction with the soil gas probes, flux chambers can be installed at the ground surface to estimate the emissions of VOCs from the subsurface. Flux chambers are inverted containers installed at the ground surface that can directly measure the emissions of VOCs from the subsurface to the atmosphere (Verginelli et al. 2018). These chambers can be used to estimate the outdoor volatilization or can be installed in buildings with exposed soil (e.g., pier-and-beam construction) or with uncracked concrete slab foundations with sealed expansion joints to quantify the vapor intrusion rate (Ma et al. 2020b). Further details on flux chambers can be found in Chap. 5.

6.3.4 Indoor Air Sampling

Measuring indoor air is the most direct approach for vapor intrusion to provide the indoor concentrations needed for risk assessment. Indoor air sampling is typically performed using passivated stainless-steel canisters with sampling periods of 24 and 8 h for residential and industrial buildings, respectively (U.S. EPA 2015a). The

samples are then sent to the laboratory for the VOCs analyses providing a time-weighted indoor concentration for the contaminants of concern averaged over the sampling period. Alternatively, passive sampling (e.g., passive sorbent sampler) can be performed, allowing a long sample collection time (days to weeks) that can reduce the effects of short-term temporal variability by yielding a time-integrated average VOC concentration (McHugh et al. 2017).

The above methods provide information on the average inhalation exposure needed to calculate long-term chronic risks. To evaluate short-term acute risks or episodic potential threats to safety (e.g., explosive concentrations of petroleum vapors or methane), alternative methods were recently developed. These include high-frequency indoor gas chromatograph-mass spectrometer (GC-MS) measurements (e.g., Gorder and Dettenmaier 2011; Beckley et al. 2014) eventually coupled with concurrent measurement of dynamic controlling factors (e.g., Kram et al. 2019, 2020) or manipulation of indoor-outdoor pressure conditions (building pressure cycling method) to measure changes in indoor air VOC concentration under positive or negative indoor air pressure (e.g., McHugh et al. 2012). High-frequency indoor GC-MS measurements are typically performed with field-portable instruments designed for on-site analysis that allow measuring indoor air VOC concentrations in almost real-time (a few minutes) during the course of the field investigation (Gorder and Dettenmaier 2011). Continuous monitoring enables the collection of a large volume of contaminant concentration data over time (tens of analyses per day), thus allowing to evaluate short-term indoor air concentration variations and the presence of background VOCs sources (Beckley et al. 2014). By coupling this analysis with simultaneous monitoring with dedicated detectors of additional parameters such as sub-foundation pressure, wind speed and barometric pressure could help to determine the cause of the vapor intrusion (Kram et al. 2019, 2020).

Building pressure cycling (BPC) is a technique that manipulates building air pressure and ventilation to promote or inhibit the intrusion of vapors into the building using either blower doors or by manipulation of existing HVAC systems (McHugh et al. 2012). Indoor air VOC concentrations are then measured either using real-time monitoring or by traditional indoor sampling after three to five times the air volume of the building has been flushed (Lutes et al. 2019). BPC reduces the spatial and temporal variability of indoor air and allows to determine the reasonable maximum exposure (RME) under negative building pressure for the assessment of short-term risks and allows to determine the presence of background sources under positive pressure conditions (McHugh et al. 2012).

Regarding the latter aspect, for the evaluation and eventual management of the vapor intrusion pathway, particular caution should be paid to identify all the potential indoor and outdoor VOCs sources (usually indicated as background) that are not related to the subsurface source of vapors (Rago et al. 2021). As discussed by U.S. EPA (2015b), indoor air in many buildings can indeed contain detectable levels of a number of VOCs associated with the use and storage of consumer products (e.g., cleaners, air fresheners, scented candles, or other household products), combustion processes (e.g., smoking, cooking, and home heating) and releases from interior building materials (e.g., carpets, paint, and wood-finishing products). Furthermore,

in urban centers, outdoor ambient concentrations of some VOCs (e.g., benzene) may exceed allowable indoor risk-based levels, as a result of vehicle traffic emissions. For the above reasons, as suggested by U.S. EPA (2015b), indoor air sampling should always be carried out in conjunction with other lines of evidence (e.g., soil gas sampling), eventually coupled with compound-specific isotope analysis (CSIA). CSIA (Chap. 11) provides an independent line of evidence to distinguish between vapor intrusion and indoor sources of VOCs by analyzing the isotope fractionation in indoor air and soil gas samples (Beckley et al. 2016). For PHCs, the isotopes to be used are ^{13}C and ^2H . The isotope composition of VOCs originating from the subsurface is often clearly different than that of pristine manufactured products acting as indoor sources of the same VOCs, and thus, this difference allows the differentiation between VOCs from indoor sources and those from true vapor intrusion sources (McHugh et al. 2011).

6.3.5 Risk Assessment

The measured or estimated indoor concentrations, C_{indoor} (g/m^3), for the different target compounds are then used in the risk assessment to establish the need for mitigation actions of the vapor intrusion pathway.

According to the risk-based corrective action (RBCA) procedure outlined in the ASTM (2000) standard, the carcinogenic and non-carcinogenic risks can be estimated as shown in Eq. 6.28:

$$\begin{cases} R = C_{\text{indoor}} \cdot \text{IUR} \cdot \text{EC} \text{ (carcinogenic effects)} \\ \text{HQ} = C_{\text{indoor}} \cdot \frac{\text{EC}}{\text{RfC}} \text{ (non - carcinogenic effects)} \end{cases} \quad (6.28)$$

where R (–) is the carcinogenic risk, HQ (–) is the hazard quotient for toxic effects, and RfC (g/m^3) and IUR (m^3/g) are the reference concentration and the inhalation unit risk that represent the toxicological parameters for toxic and carcinogenic effects (see Table 6.4). EC (–) is the exposure factor that can be estimated as in Eq. 6.29:

$$\text{EC} = \frac{\text{EF}_{\text{gi}} \cdot \text{EF} \cdot \text{ED}}{\text{BW} \cdot \text{AT} \cdot 365 \frac{\text{days}}{\text{year}} \cdot 24 \frac{\text{hours}}{\text{day}}} \quad (6.29)$$

where BW (kg) is the body weight, EF (d/y) is the annual exposure frequency, EF_{gi} (h/d) the daily exposure frequency, ED (y) is the exposure duration, and AT (y) is the averaging time (set equal to ED for the toxic effects).

The above equations can be rearranged as in Eq. 6.30 to calculate the acceptable indoor risk-based levels, $C_{\text{indoor,acc}}$ (g/m^3), that ensure the target risk, TR (–), and hazard quotient, THQ (–):

Table 6.4 Toxicological parameters (U.S. EPA 2020) and example of indoor risk-based concentration for some petroleum compounds of concern for petroleum vapor intrusion. The acceptable indoor risk-based levels ($C_{\text{indoor,acc}}$) were calculated using the following parameters: $TR = 10^{-6}$, $THQ = 1$, $BW = 70$ kg, $EF = 350$ d/y, $EF_{\text{gi}} = 24$ h/d, $ED = 30$ y, $AT = ED$ for toxic effects, $AT = 70$ y for carcinogenic effects

Compound	RfC	IUR	$C_{\text{indoor,acc}}$
	(mg/m^3)	($\mu\text{g}/\text{m}^3$) ⁻¹	($\mu\text{g}/\text{m}^3$)
Benzene	0.03	7.80×10^{-6}	0.31
Toluene	5	–	5214
Ethylbenzene	1	2.50×10^{-6}	0.97
Xylenes	0.1	–	104
Naphthalene	0.003	3.40×10^{-5}	0.072

$$C_{\text{indoor,acc}} = \min \left\{ \begin{array}{l} \frac{TR}{IUR \cdot EC} \text{ (carcinogenic effects)} \\ \frac{THQ \cdot RfC}{EC} \text{ (non - carcinogenic effects)} \end{array} \right. \quad (6.30)$$

Table 6.4 reports an example of the indoor risk-based concentrations calculated with the above equations for some petroleum compounds typically of concern for petroleum vapor intrusion, assuming a target cancer risk level of one per million (10^{-6}) and a target hazard quotient of 1 for non-carcinogenic effects. The assumed exposure factors were: $BW = 70$ kg, $EF = 350$ d/y, $EF_{\text{gi}} = 24$ h/d, $ED = 30$ y, $AT = ED$ for toxic effects and $AT = 70$ y for carcinogenic effects.

As discussed earlier, benzene is usually the most critical compound for vapor intrusion although as shown by Brewer et al. (2013) when benzene is less than approximately 1% in the hydrocarbon mixture (i.e., when the concentration of TPH is more than 900 times that of benzene) TPH could drive vapor intrusion risk (for C5–C8 and C9–C12 aliphatics).

6.4 Conclusions

Although there were significant advances in PVI science over the last decades, knowledge gaps still exist. Regarding the vapor intrusion route, the importance of sewers or other utility tunnels as preferential pathways for VOC migration into buildings has received increased focus in recent years (Ma et al. 2020a), but their understanding, especially in the case of petroleum vapors, is very limited. Bubble-facilitated transport above NAPL sources is also attracting attention, but more field and laboratory studies are still required to understand the significance of this pathway. The role of pervious slabs for PVI is another aspect that could be addressed in the future as diffusive transport through permeable concrete slabs can enhance the oxygen availability

in the subsurface (U.S. EPA 2015a), thus creating conditions favorable for the occurrence of aerobic biodegradation even below large buildings (Verginelli et al. 2016a). Finally, considering that most of the field experience was gained in the United States and, for some aspects (e.g., vertical distance criteria), also in Australia, future studies could be oriented to evaluate if the criteria and approaches adopted in these countries should be modulated to account for difference in types of building construction, climate, or geological settings.

Regarding soil gas and indoor sampling, in the last decade, there was increasing attention in developing and testing new methods to account for the dynamics of vapor intrusion and determine the presence of indoor background sources. These methods include real-time GC–MS analysis eventually coupled with concurrent measurement of dynamic controlling factors (e.g., sub-foundation pressure, wind speed, and barometric pressure), building pressure cycling methods to measure changes in indoor air VOC concentration under positive or negative indoor air pressure, quantitative passive soil gas sampling, and CSIA. The further development and refinement of these methods along with a better understanding of the fate and transport of petroleum vapors in the subsurface will trace the path for a better understanding and management of petroleum vapor intrusion.

References

- Abreu LD, Johnson PC (2006) Simulating the effect of aerobic biodegradation on soil vapor intrusion into buildings: influence of degradation rate, source concentration, and depth. *Environ Sci Technol* 40(7):2304–2315. <https://doi.org/10.1021/es051335p>
- Abreu LD, Ettinger R, McAlary T (2009) Simulated soil vapor intrusion attenuation factors including biodegradation for petroleum hydrocarbons. *Ground Water Monit Remediat* 29(1):105–117. <https://doi.org/10.1111/j.1745-6592.2008.01219.x>
- Abreu LD, Schuver H (2012) Conceptual model scenarios for the vapor intrusion pathway. EPA 530-R-10-003. USEPA Office of Resource Conservation and Recovery, Washington, DC. www.epa.gov/sites/production/files/2015-09/documents/vi-cms-v11final-2-24-2012.pdf. Accessed Dec 2021
- Abreu LD, Lutes CC, Nichols EM (2013) 3-D modeling of aerobic biodegradation of petroleum vapors: effect of building area size on oxygen concentration below the slab. Office of Underground Storage Tanks (OUST). EPA 510-R-13-002. <http://www.epa.gov/oust/cat/pvi/building-size-modeling.pdf>. Accessed Dec 2021
- Amos RT, Mayer KU, Bekins BA, Delin GN, Williams RL (2005) Use of dissolved and vapor-phase gases to investigate methanogenic degradation of petroleum hydrocarbon contamination in the subsurface. *Water Resour Res* 41(2). <https://doi.org/10.1029/2004WR003433>
- Amos RT, Mayer KU (2006) Investigating ebullition in a sand column using dissolved gas analysis and reactive transport modeling. *Environ Sci Technol* 40(17):5361–5367. <https://doi.org/10.1021/es0602501>
- API (2017) Quantification of vapor phase-related natural source zone depletion processes. American Petroleum Institute, Publication No. 4784. Available at <http://www.api.org>
- ASTM (2000) Standard guide for risk-based corrective action. ASTM, West Conshohocken, PA, E2081-00. Accessed Dec 2021

- Beckley L, Gorder K, Dettenmaier E, Rivera-Duarte I, McHugh T (2014) On-site gas chromatography/mass spectrometry (GC/MS) analysis to streamline vapor intrusion investigations. *Environ Forensics* 15(3):234–243. <https://doi.org/10.1080/15275922.2014.930941>
- Beckley L, McHugh T, Philp P (2016) Utility of compound-specific isotope analysis for vapor intrusion investigations. *Ground Water Monit Remediat* 36(4):31–40. <https://doi.org/10.1111/gwmr.12185>
- Beckley L, McHugh T (2020) A conceptual model for vapor intrusion from groundwater through sewer lines. *Sci Total Environ* 698:134283. <https://doi.org/10.1016/j.scitotenv.2019.134283>
- Bekele DN, Naidu R, Bowman M, Chadalavada S (2013) Vapor intrusion models for petroleum and chlorinated volatile organic compounds: opportunities for future improvements. *Vadose Zone J* 12(2). <https://doi.org/10.2136/vzj2012.0048>
- Brewer R, Nagashima J, Kelley M, Heskett M, Rigby M (2013) Risk-based evaluation of total petroleum hydrocarbons in vapor intrusion studies. *Int J Environ Res Public Health* 10(6):2441–2467. <https://doi.org/10.3390/ijerph10062441>
- Brewer R, Nagashima J, Rigby M, Schmidt M, O'Neill H (2014) Estimation of generic subsurface attenuation factors for vapor intrusion investigations. *Ground Water Monit Remediat* 34(4):79–92. <https://doi.org/10.1111/gwmr.12086>
- CRC CARE (2013) Petroleum hydrocarbon vapour intrusion assessment: Australian guidance. CRC CARE Technical Report no. 23, CRC for Contamination Assessment and Remediation of the Environment, Adelaide, Australia. www.crccare.com/publications/technical-reports. Accessed Dec 2021
- Davis GB, Patterson BM, Trefry MG (2009a) Evidence for instantaneous oxygen-limited biodegradation of petroleum hydrocarbon vapors in the subsurface. *Ground Water Monit Remediat* 29(1):126–137. <https://doi.org/10.1111/j.1745-6592.2008.01221.x>
- Davis GB, Patterson BM, Trefry MG (2009b) Biodegradation of petroleum hydrocarbon vapours. CRC CARE 2009b, Technical Report no. 12, CRC for Contamination Assessment and Remediation of the Environment, Adelaide, Australia. www.crccare.com/publications/technical-reports. Accessed Dec 2021
- DeVaul GE, Ettinger RA, Salanitro JP, Gustafson JB (1997) Benzene, toluene, ethylbenzene, and xylenes (BTEX) degradation in vadose zone soils during vapor transport: first-order rate constants (No. CONF-971116-). Ground Water Publishing Co., Westerville, OH (United States)
- DeVaul GE (2007) Indoor vapor intrusion with oxygen-limited biodegradation for a subsurface gasoline source. *Environ Sci Technol* 41(9):3241–3248. <https://doi.org/10.1021/es060672a>
- DeVaul GE, McHugh TE, Newberry P (2010) Users' manual "Bio vapor: a 1-D vapor intrusion model with oxygen-limited aerobic biodegradation"; American Petroleum Institute, Washington, DC. <https://www.api.org/oil-and-natural-gas/environment/clean-water/ground-water/vapor-intrusion/bio-vapor>. Accessed Dec 2021
- DeVaul GE (2011) Biodegradation rates for petroleum hydrocarbons in aerobic soils: a summary of measured data. In: International symposium on bioremediation and sustainable environmental technologies. Reno, NV
- DeVaul GE, Rhodes IA, Hinojosa E, Bruce CL (2020) Petroleum NAPL depletion estimates and selection of marker constituents from compositional analysis. *Ground Water Monit Remediat* 40(4):44–53. <https://doi.org/10.1111/gwmr.12410>
- Eklund B (2016) Effect of environmental variables on vapor transport. In: Proceedings of the 26th annual international conference on soil, water, energy, and air, San Diego, CA
- Flintoft L (2003) Boost for bacterial batteries. *Nat Rev Microbiol* 1(2):88–88. <https://doi.org/10.1038/nrmicro758>
- Fuchs G, Boll M, Heider J (2011) Microbial degradation of aromatic compounds—from one strategy to four. *Nat Rev Microbiol* 9(11):803–816. <https://doi.org/10.1038/nrmicro2652>
- Garg S, Newell CJ, Kulkarni PR, King DC, Adamson DT, Renno MI, Sale T (2017) Overview of natural source zone depletion: processes, controlling factors, and composition change. *Ground Water Monit Rem* 37(3):62–81. <https://doi.org/10.1111/gwmr.12219>

- Górecki T, Namiesnik J (2002) Passive sampling. *Trends Analyt Chem* 21:276–291. [https://doi.org/10.1016/S0165-9936\(02\)00407-7](https://doi.org/10.1016/S0165-9936(02)00407-7)
- Gorder KA, Dettenmaier EM (2011) Portable GC/MS methods to evaluate sources of cVOC contamination in indoor air. *Ground Water Monit Remediat* 31(4):113–119. <https://doi.org/10.1111/j.1745-6592.2011.01357.x>
- Gschwend P, MacFarlane J, Jensen D, Soo J, Sapparaiuly G, Borrelli R, Vago F, Oldani A, Zaninetta L, Verginelli I, Baciocchi R (2022) In situ equilibrium polyethylene passive sampling of soil gas VOC concentrations: modeling, parameter determinations, and laboratory testing. *Environ Sci Technol*. <https://doi.org/10.1021/acs.est.1c07045>
- Hers I, Atwater J, Li L, Zapf-Gilje R (2000) Evaluation of vadose zone biodegradation of BTX vapours. *J Contam Hydrol* 46(3–4):233–264. [https://doi.org/10.1016/S0169-7722\(00\)00135-2](https://doi.org/10.1016/S0169-7722(00)00135-2)
- Hers I, Zapf-Gilje R, Johnson PC, Li L (2003) Evaluation of the Johnson and Ettinger model for prediction of indoor air quality. *Ground Water Monit Rem* 23(2):119–133. <https://doi.org/10.1111/j.1745-6592.2003.tb00678.x>
- Hers I, Jourabchi P, Lahvis MA, Dahlen P, Luo EH, Johnson PC, Mayer KU (2014) Evaluation of seasonal factors on petroleum hydrocarbon vapor biodegradation and intrusion potential in a cold climate. *Ground Water Monit Rem* 34(4):60–78. <https://doi.org/10.1111/gwmr.12085>
- Hodny JW, Whetzel Jr JE, Anderson II HS (2009) Quantitative passive soil gas and air sampling in vapor intrusion investigations. In: Proceedings of the AW&MA vapor intrusion 2009 conference
- Illangasekare T, Petri B, Fucik R, Sauck C, Shannon L, Sakaki T, Smits K, Cihan A, Christ J, Schulte P (2014) Vapor intrusion from entrapped NAPL sources and groundwater plumes: process understanding and improved modeling tools for pathway assessment. Colorado School of Mines Golden. <https://clu-in.org/download/issues/vi/VI-ER-1687-FR.pdf>. Accessed Dec 2021
- ITRC (2009) Evaluation of natural source zone depletion at sites with LNAPL. Interstate Technology and Regulatory Council, LNAPL Team, Washington, DC, April 2009. <https://www.itrcweb.org/guidancedocuments/lnapl-1.pdf>. Accessed Dec 2021
- ITRC (2014) Petroleum vapor intrusion: fundamentals of screening, investigation, and management. Interstate Technology and Regulatory Council, Vapor Intrusion Team, Washington, DC, October 2014. <https://projects.itrcweb.org/PetroleumVI-Guidance/>. Accessed Dec 2021
- ITRC (2018) Light non-aqueous phase liquids (LNAPL) document update, LNAPL-3. Interstate Technology & Regulatory Council, LNAPL Update Team, Washington, USA. <https://lnapl-3.itrcweb.org/>. Accessed Dec 2021
- Johnson PC, Ettinger RA (1991) Heuristic model for predicting the intrusion rate of contaminant vapors into buildings. *Environ Sci Technol* 25(8):1445–1452. <https://doi.org/10.1021/es00020a013>
- Knight JH, Davis GB (2013) A conservative vapour intrusion screening model of oxygen-limited hydrocarbon vapour biodegradation accounting for building footprint size. *J Contam Hydrol* 155:46–54. <https://doi.org/10.1016/j.jconhyd.2013.09.005>
- Kram ML, Hartman B, Clite N (2019) Automated continuous monitoring and response to toxic subsurface vapors entering overlying buildings—selected observations, implications and considerations. *Remed J* 29(3):31–38. <https://doi.org/10.1002/rem.21605>
- Kram ML, Hartman B, Frescura C, Negrao P, Egelton D (2020) Vapor intrusion risk evaluation using automated continuous chemical and physical parameter monitoring. *Remed J* 30(3):65–74. <https://doi.org/10.1002/rem.21646>
- Lahvis MA, Hers I, Davis RV, Wright J, DeVuall GE (2013) Vapor intrusion screening at petroleum UST sites. *Ground Water Monit Rem* 33(2):53–67. <https://doi.org/10.1111/gwmr.12005>
- Lahvis MA, Ettinger RA (2021) Improving risk-based screening at vapor intrusion sites in California. *Ground Water Monit Rem* 41(2):73–86. <https://doi.org/10.1111/gwmr.12450>
- Liang C, Chang JS, Chen TW, Hou Y (2020) Passive membrane sampler for assessing VOCs contamination in unsaturated and saturated media. *J Hazard Mater* 401:123387. <https://doi.org/10.1016/j.jhazmat.2020.123387>
- Liu X, Ma E, Zhang YK, Liang X (2021) An analytical model of vapor intrusion with fluctuated water table. *J Hydrol* 596:126085. <https://doi.org/10.1016/j.jhydrol.2021.126085>

- Lutes CC, Holton CW, Truesdale R, Zimmerman JH, Schumacher B (2019) Key design elements of building pressure cycling for evaluating vapor intrusion—a literature review. *Ground Water Monit Rem* 39(1):66–72. <https://doi.org/10.1111/gwmr.12310>
- Ma E, Zhang YK, Liang X, Yang J, Zhao Y, Liu X (2019) An analytical model of bubble-facilitated vapor intrusion. *Water Res* 165:114992. <https://doi.org/10.1016/j.watres.2019.114992>
- Ma J, Rixey WG, DeVaul GE, Stafford BP, Alvarez PJ (2012) Methane bioattenuation and implications for explosion risk reduction along the groundwater to soil surface pathway above a plume of dissolved ethanol. *Environ Sci Technol* 46(11):6013–6019. <https://doi.org/10.1021/es300715f>
- Ma J, McHugh T, Beckley L, Lahvis MA, DeVaul GE, Jiang L (2020a) Vapor intrusion investigations and decision-making: a critical review. *Environ Sci Technol* 54(12):7050–7069. <https://doi.org/10.1021/acs.est.0c00225>
- Ma J, McHugh T, Eklund B (2020b) Flux chamber measurements should play a more important role in contaminated site management. *Environ Sci Technol* 54(19):11645–11647. <https://doi.org/10.1021/acs.est.0c04078>
- McAlary T, Wang X, Unger A, Groenevelt H, Górecki T (2014) Quantitative passive soil vapor sampling for VOCs—part I: theory. *Environ Sci Process Impacts* 16(3):482–490. <https://doi.org/10.1039/C3EM00652B>
- McCoy K, Zimbron J, Sale T, Lyverse M (2014) Measurement of natural losses of LNAPL using CO₂ traps. *Groundwater* 53(4):658–667. <https://doi.org/10.1111/gwat.12240>
- McHugh TE, McAlary T (2009) Important physical processes for vapor intrusion: a literature review. In: *Proceedings of AWMA vapor intrusion conference, San Diego, CA*
- McHugh TE, Davis R, DeVaul GE, Hopkins H, Menatti J, Peargin T (2010) Evaluation of vapor attenuation at petroleum hydrocarbon sites: considerations for site screening and investigation. *Soil Sediment Contam* 19(6):725–745. <https://doi.org/10.1080/15320383.2010.499923>
- McHugh TE, Kuder T, Fiorenza S, Gorder K, Dettenmaier E, Philp P (2011) Application of CSIA to distinguish between vapor intrusion and indoor sources of VOCs. *Environ Sci Technol* 45(14):5952–5958. <https://doi.org/10.1021/es200988d>
- McHugh TE, Beckley L, Bailey D, Gorder K, Dettenmaier E, Rivera-Duarte I, MacGregor IC (2012) Evaluation of vapor intrusion using controlled building pressure. *Environ Sci Technol* 46(9):4792–4799. <https://doi.org/10.1021/es204483g>
- McHugh TE, Loll P, Eklund B (2017) Recent advances in vapor intrusion site investigations. *J Environ Manage* 204:783–792. <https://doi.org/10.1016/j.jenvman.2017.02.015>
- Millington RJ, Quirk JP (1961) Permeability of porous solids. *Trans Faraday Soc* 57:1200–1207
- Molins S, Mayer KU, Amos RT, Bekins BA (2010) Vadose zone attenuation of organic compounds at a crude oil spill site—interactions between biogeochemical reactions and multicomponent gas transport. *J Contam Hydrol* 112(1–4):15–29. <https://doi.org/10.1016/j.jconhyd.2009.09.002>
- Nielsen KB, Hvidberg B (2017) Remediation techniques for mitigating vapor intrusion from sewer systems to indoor air. *Remed J* 27(3):67–73. <https://doi.org/10.1002/rem.21520>
- Parker JC (2003) Modeling volatile chemical transport, biodecay, and emission to indoor air. *Ground Water Monit Rem* 23(1):107–120. <https://doi.org/10.1111/J.1745-6592.2003.TB00789.X>
- Rago R, Rezendes A, Peters J, Chatterton K, Kammari A (2021) Indoor air background levels of volatile organic compounds and air-phase petroleum hydrocarbons in office buildings and schools. *Ground Water Monit Rem* 41(2):27–47. <https://doi.org/10.1111/gwmr.12433>
- Ririe GT, Sweeney RE, Daugherty SJ (2002) A comparison of hydrocarbon vapor attenuation in the field with predictions from vapor diffusion models. *Soil Sediment Contam* 11(4):529–554. <https://doi.org/10.1080/20025891107159>
- Rivett MO, Wealthall GP, Dearden RA, McAlary TA (2011) Review of unsaturated-zone transport and attenuation of volatile organic compound (VOC) plumes leached from shallow source zones. *J Contam Hydrol* 123(3–4):130–156. <https://doi.org/10.1016/j.jconhyd.2010.12.013>
- Roghani M, Jacobs OP, Miller A, Willett EJ, Jacobs JA, Viteri CR, Pennell KG (2018) Occurrence of chlorinated volatile organic compounds (VOCs) in a sanitary sewer system: Implications for

- assessing vapor intrusion alternative pathways. *Sci Total Environ* 616:1149–1162. <https://doi.org/10.1016/j.scitotenv.2017.10.205>
- Salim F, Górecki T (2019) Theory and modelling approaches to passive sampling. *Environ Sci Process Impacts* 21(10):1618–1641. <https://doi.org/10.1039/C9EM00215D>
- Shen R, Pennell KG, Suuberg EM (2013) Influence of soil moisture on soil gas vapor concentration for vapor intrusion. *Environ Eng Sci* 30(10):628–637. <https://doi.org/10.1089/ees.2013.0133>
- Sihota NJ, Mayer KU, Toso MA, Atwater JF (2013) Methane emissions and contaminant degradation rates at sites affected by accidental releases of denatured fuel-grade ethanol. *J Contam Hydrol* 151:1–15. <https://doi.org/10.1016/j.jconhyd.2013.03.008>
- Song S, Ramacciotti FC, Schnorr BA, Bock M, Stubbs CM (2011) Evaluation of USEPA's empirical attenuation factor database. Air Waste and Management Association. Emissions Monitoring, 16–21 Feb 2011
- Soucy NC, Mumford KG (2017) Bubble-facilitated VOC transport from LNAPL smear zones and its potential effect on vapor intrusion. *Environ Sci Technol* 51(5):2795–2802. <https://doi.org/10.1021/acs.est.6b06061>
- Tillman FD, Weaver JW (2005) Review of recent research on vapor intrusion. Washington, DC 20460: US Environmental Protection Agency, Office of Research and Development
- Tillman FD, Weaver JW (2007) Temporal moisture content variability beneath and external to a building and the potential effects on vapor intrusion risk assessment. *Sci Total Environ* 379(1):1–15. <https://doi.org/10.1016/j.scitotenv.2007.02.003>
- Unnithan A, Bekele D, Chadalavada S, Naidu R (2021) Insights into vapour intrusion phenomena: current outlook and preferential pathway scenario. *Sci Total Environ* 796:148885. <https://doi.org/10.1016/j.scitotenv.2021.148885>
- U.S. EPA (1995) Light nonaqueous-phase liquids. EPA/540/S-95/500. EPA Groundwater Issue. <http://nepis.epa.gov/Exe/ZyPURL.cgi?Dockey=10002DXR.txt>. Accessed Dec 2021
- U.S. EPA (2002) OSWER draft guidance for evaluating the vapor intrusion to indoor air pathway from groundwater and soils (Subsurface Vapor Intrusion Guidance). Office of Solid Waste and Emergency Response, Washington, D.C. EPA530-D-02-004. <https://nepis.epa.gov/Exe/ZyPURL.cgi?Dockey=P1008OTB.TXT>. Accessed Dec 2021
- U.S. EPA (2013) Evaluation of empirical data and modeling studies to support soil vapor intrusion screening criteria for petroleum hydrocarbon compounds. EPA 510-R-13-001. Washington, DC: U.S. Environmental Protection Agency, Office of Solid Waste and Emergency Response. https://www.epa.gov/sites/default/files/2014-09/documents/pvi_database_report.pdf. Accessed Dec 2021
- U.S. EPA (2015a) Technical guide for addressing petroleum vapor intrusion at leaking underground storage tank sites. Office of Underground Storage Tanks (OUST). EPA 510-R-15-001, 2015a. <http://www.epa.gov/oust/cat/pvi/pvi-guide-final-6-10-15.pdf>. Accessed Dec 2021
- U.S. EPA (2015b) OSWER technical guide for assessing and mitigating the vapor intrusion pathway from subsurface vapor sources to indoor air. OSWER Publication 9200.2-154. U.S. Environmental Protection Agency, Office of Solid Waste and Emergency Response, June 2015. <https://www.epa.gov/sites/production/files/2015-09/documents/oswer-vapor-intrusion-technical-guide-final.pdf>. Accessed Dec 2021
- U.S. EPA (2017) Documentation for EPA's implementation of the Johnson and Ettinger model to evaluate site specific vapor intrusion into buildings. Office of Superfund Remediation and Technology Innovation, Washington, DC. <https://semspub.epa.gov/work/HQ/10000489.pdf>. Accessed Dec 2021
- U.S. EPA (2018) Update for Chapter 19 of the exposure factors handbook. EPA/600/R-18/121F. <https://cfpub.epa.gov/ncea/risk/recordisplay.cfm?deid=340635>. Accessed Dec 2021
- U.S. EPA (2020) Toxicity and chemical/physical properties for Regional screening level (RSL) of chemical contaminants at superfund sites. U.S. Environmental Protection Agency, Region 9 May 2020. <http://www.epa.gov/region9/superfund/prg/>. Accessed Dec 2021

- Van Genuchten MT (1980) A closed-form equation for predicting the hydraulic conductivity of unsaturated soils. *Soil Sci Soc Am J* 44 (5):892–898. <https://doi.org/10.2136/sssaj1980.03615995004400050002x>
- Verginelli I, Baciocchi R (2021) Refinement of the gradient method for the estimation of natural source zone depletion at petroleum contaminated sites. *J Contam Hydrol* 241:103807. <https://doi.org/10.1016/j.jconhyd.2021.103807>
- Verginelli I, Baciocchi R (2014) Vapor intrusion screening model for the evaluation of risk-based vertical exclusion distances at petroleum contaminated sites. *Environ Sci Technol* 48(22):13263–13272. <https://doi.org/10.1021/es503723g>
- Verginelli I, Yao Y, Wang Y, Ma J, Suuberg EM (2016a) Estimating the oxygenated zone beneath building foundations for petroleum vapor intrusion assessment. *J Hazard Mater* 312:84–96. <https://doi.org/10.1016/j.jhazmat.2016.03.037>
- Verginelli I, Capobianco O, Baciocchi R (2016b) Role of the source to building lateral separation distance in petroleum vapor intrusion. *J Contam Hydrol* 189:58–67. <https://doi.org/10.1016/j.jconhyd.2016.03.009>
- Verginelli I, Yao Y, Suuberg EM (2016c) An excel[®]-based visualization tool of two-dimensional soil gas concentration profiles in petroleum vapor intrusion. *Ground Water Monit Rem* 36(2):94–100. <https://doi.org/10.1111/gwmmr.12162>
- Verginelli I, Pecoraro R, Baciocchi R (2018) Using dynamic flux chambers to estimate the natural attenuation rates in the subsurface at petroleum contaminated sites. *Sci Total Environ* 619:470–479. <https://doi.org/10.1016/j.scitotenv.2017.11.100>
- Verginelli I, Yao Y (2021) A review of recent vapor intrusion modeling work. *Ground Water Monit Rem* 2:138–144. <https://doi.org/10.1111/gwmmr.12455>
- Yao Y, Shen R, Pennell KG, Suuberg EM (2013) A review of vapor intrusion models. *Environ Sci Technol* 47(6):2457–2470. <https://doi.org/10.1021/es302714g>
- Yao Y, Yang F, Suuberg EM, Provoost J, Liu W (2014) Estimation of contaminant subsurface concentration in petroleum vapor intrusion. *J Hazard Mater* 279:336–347. <https://doi.org/10.1016/j.jhazmat.2014.05.065>
- Yao Y, Wu Y, Wang Y, Verginelli I, Zeng T, Suuberg EM, Jiang L, Wen Y, Ma J (2015) A petroleum vapor intrusion model involving upward advective soil gas flow due to methane generation. *Environ Sci Technol* 49(19):11577–11585. <https://doi.org/10.1021/acs.est.5b01314>
- Yao Y, Verginelli I, Suuberg EM (2016a) A two-dimensional analytical model of petroleum vapor intrusion. *Water Resour Res* 52(2):1528–1539. <https://doi.org/10.1002/2015WR018320>
- Yao Y, Wang Y, Verginelli I, Suuberg EM, Ye J (2016b) Comparison between PVI2D and Abreu–Johnson’s model for petroleum vapor intrusion assessment. *Vadose Zone J* 15(11):1–11. <https://doi.org/10.2136/vzj2016.07.0063>
- Yao Y, Verginelli I, Suuberg EM (2017) A two-dimensional analytical model of vapor intrusion involving vertical heterogeneity. *Water Resour Res* 53(5):4499–4513. <https://doi.org/10.1002/2016WR020317>
- Yao Y, Verginelli I, Suuberg EM, Eklund B (2018) Examining the use of USEPA’s generic attenuation factor in determining groundwater screening levels for vapor intrusion. *Ground Water Monit Rem* 38(2):79–89. <https://doi.org/10.1111/gwmmr.12276>
- Yao Y, Mao F, Xiao Y, Luo J (2019) Modeling capillary fringe effect on petroleum vapor intrusion from groundwater contamination. *Water Res* 150:111–119. <https://doi.org/10.1016/j.watres.2018.11.038>

Open Access This chapter is licensed under the terms of the Creative Commons Attribution 4.0 International License (<http://creativecommons.org/licenses/by/4.0/>), which permits use, sharing, adaptation, distribution and reproduction in any medium or format, as long as you give appropriate credit to the original author(s) and the source, provide a link to the Creative Commons license and indicate if changes were made.

The images or other third party material in this chapter are included in the chapter's Creative Commons license, unless indicated otherwise in a credit line to the material. If material is not included in the chapter's Creative Commons license and your intended use is not permitted by statutory regulation or exceeds the permitted use, you will need to obtain permission directly from the copyright holder.

